Discrimination Between Benign and Malignant ProstateTissue Using ChromatinTexture Analysis in 3-D by Confocal Laser Scanning Microscopy

André Huisman,[1] Lennert S. Ploeger,[1] Hub F.J. Dullens,[1] Trudy N. Jonges,[1] Jeroen A.M. Belien,[2] Gerrit A. Meijer,[2] Neal Poulin,[1] William E. Grizzle,[3] and Paul J. van Diest[1]*

[1]Department of Pathology, University Medical Center, Utrecht, The Netherlands
[2]Department of Pathology, VU University Medical Center, Amsterdam, The Netherlands
[3]Department of Pathology, University of Alabama at Birmingham, Alabama, United States of America

BACKGROUND. Analysis of chromatin texture may improve both the diagnosis and the assessment of the prognosis of prostate cancer. Confocal laser scanning microscopy (CLSM) allows performing measurements in nuclei reconstructed in 3-D. The aim of this study was to evaluate the clinical usefulness of 3-D texture analysis of prostate tissue.
METHODS. Image stacks of eight prostate cancer sections were obtained by CLSM of both benign and malignant areas. Texture feature values were computed for individual nuclei. The discriminative power of the texture features was established by receiver operating characteristic (ROC) analysis and linear discriminant analysis (LDA).
RESULTS. Texture features were identified that could discriminate between benign and malignant nuclei. LDA correctly classified 89% of the nuclei of the pooled set of benign and malignant nuclei.
CONCLUSIONS. 3-D nuclear texture features allow discrimination of most benign and malignant prostate nuclei. We estimate that the classification rates can be increased by improving the image quality. *Prostate 67: 248–254, 2007.*

KEY WORDS: **confocal laser scanning microscopy; 3-D; texture features; image analysis; prostate cancer; DNA ploidy**

INTRODUCTION

The transformation of a normal cell to a malignant cell is associated with genetic alterations that often result in aberrant chromosome sets (''aneuploidy'') and morphological changes in the nucleus [1]. Nuclear DNA content can be assessed by, for example, image [2] or flow cytometry [3] or by comparative genomic hybridization. The morphological changes concern increased nuclear size, presence of and increased size of nucleoli and aberrant chromatin distribution patterns [4,5]. The nuclear chromatin distribution in genetically altered cells is generally coarsely-clumped with multiple chromacenters and larger nucleoli as opposed to finely granular with few chromacenters and no or small nucleoli in normal cells. These changes are often rather subtle or even subvisible, and are referred to as ''malignancy associated changes'' as they may be detected in morphologically benign cells as well [2]. They are therefore best not visually assessed but mathematically quantified as ''texture features'' that are very sensitive and not prone to observer subjectivity.

There is a vast amount of literature on the clinical value of the assessment of DNA content and nuclear texture features by image analysis in conventional prostate tissue sections [6,7] or cytospins prepared

finom

durván csomósodott

*Correspondence to: Prof. Paul J. van Diest, Department of Pathology, University Medical Center Utrecht, PO Box 85500, 3508 GA Utrecht, The Netherlands. E-mail: p.j.vandiest@umcutrecht.nl
Received 2 March 2006; Accepted 25 May 2006
DOI 10.1002/pros.20507
Published online 30 October 2006 in Wiley InterScience (www.interscience.wiley.com).

from prostate cell suspensions [8]. These assessments have already been used for computer-aided diagnosis, and prognosis [9,10]. DNA non-diploidy [11] and several nuclear texture features [12] are strong indicators of poor prognosis of prostate cancer. Using conventional tissue sections in bright-field microscopy has the drawback that only a thin slice (typical 3–4 μm) of the nucleus is imaged with subsequent loss of information. This is avoided by preparing cytospins from cell suspensions, but this introduces artifacts by the flattening of nuclei while spinning them down at high speed. Furthermore, the morphological context of the analyzed nuclei is completely lost by the dissociation process. These drawbacks can be completely avoided by using the ability to image thick sections (typical 10–50 μm) by confocal laser scanning microscopy (CLSM). Thin optical slices are acquired at high resolution by confocal imaging, and these are subsequently reconstructed in 3-D [13]. In previous studies we have described 3-D segmentation procedures [14], established the required nuclear sample size to achieve proper 3-D DNA histogram quality [15], developed an optimal tissue processing technique for 3-D CLSM [16], and described the successful software implementation of 3-D nuclear texture features [17]. The aim of this study was to perform a first evaluation of the clinical usefulness of 3-D nuclear DNA content and texture analysis in prostatectomy specimens containing prostate cancer.

MATERIALS AND METHODS

Tissue Preparation

Fourteen-micron thick sections were cut from representative paraffin-embedded tissue blocks of eight prostatectomy specimens containing prostate cancer. Our previously developed protocol was used for staining: incubation with RNase-A for 1 hr and staining with the stoichiometric dye TO-PRO-3 (Molecular Probes, Eugene, OR) iodide (633 nm excitation, maximum emission at 661 nm) in a concentration of 1:2,200 for 2 hr at room temperature [18]. After rinsing with distilled water the tissues were mounted in Vectashield (Vector Laboratories, Burlingame, CA) and sealed with a coverslip.

Image Acquisition and Analysis

Image stacks were acquired with a confocal microscope (using a Leica TCS SP2 AOBS, Leica Microsystems, Heidelberg, Germany) fitted with 100×/1.40 NA oil immersion objective. The depth information was oversampled to obtain (almost) square voxels. Resolution at the specimen level was $0.292 \times 0.292 \times 0.285\ \mu m^3$ and the dynamic range was 12 bits. A pathologist (PvD) selected and marked benign and malignant regions on an H&E stained tissue section, parallel to the TO-PRO-3 stained tissue section. To obtain measurements for at least 300 nuclei as previously set [15], 12 image stacks ($150\ \mu m^2$) were acquired. The different image stacks were selected approximately 350 μm apart to avoid potential bleaching of neighboring fields during image acquisition. The x-y co-ordinates of each field were stored using in-house developed add-on software for the confocal microscope. These co-ordinates were used for automated acquisition of the defined fields. The bottom and top of the defined fields were identified interactively as the slices where the number of (cut) nuclei was very low [14]. Stacks of approximately 120 2-D digital images (512×512 pixels) were obtained, depending on the effective thickness of the tissue.

The image stacks were segmented and analyzed off-line using in-house developed software, as described previously [14]. Segmentation was stopped when 300 nuclei were collected [15].

The DNA content of all individual nuclei was depicted in DNA histograms (50 bins, scaling to 10c). The co-efficient of variation (CV) of the DNA histogram was computed as a quality measure of the DNA distribution with the MultiCycle software program (Phoenix Flow Systems, San Diego, CA) as described previously and DNA ploidy status was noted [19]. DNA histograms obtained by conventional 2-D image cytometry according to the ESACP guidelines [20] were interpreted similarly.

Oncol

Texture Feature Computation

Our in-house developed software for the computation of 35 texture features was used as described before [17]. This software computes for every segmented nucleus the 35 scalar texture feature values. In short, the selected texture features are from three different classes: discrete features, Markovian features, fractal features. General descriptive statistical features of the gray-value distribution were computed as well [21]. Discrete texture features summarize several general statistics for the different chromatin condensation states in the nucleus, corresponding to different gray-values ranges. The Markovian features involve second order gray level statistics and are computed from co-occurrence matrices, representing the joint probability that pairs of gray-level combinations they co-occur together. Several statistics can be computed from those matrices: heuristic features, statistical features, and features taken from information theory [22]. Fractals are mathematical objects which have similar details on every scale. Fractals have a strong correlation with human judgment of texture roughness [23].

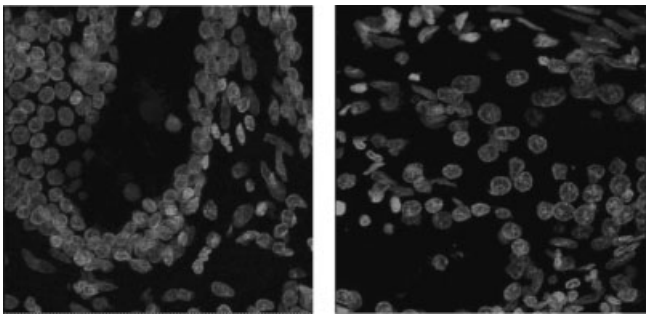

Fig. 1. Representative examples of a maximum intensity projection of a benign (**left**) and a malignant (**right**) image stack of prostate tissue stained with TO-PRO-3, acquired by CLSM, imaged with a 100×/1.40 NA oil immersion objective.

Data Analysis

The 3-D DNA histograms were compared to the 2-D histograms with regard to DNA ploidy and CV.

Two approaches were used to evaluate the discriminative power of the texture features for benign and malignant nuclei. First, receiver operating characteristic (ROC) curves were plotted for each feature as a graphical representation of the trade off between the false negative and false positive rates. Discriminative texture features were defined to have an area under the curve (AUC) of 0.5–1, but features with an AUC > 0.80 were considered to have good discriminative power.

Further, multivariate linear discriminant analysis (LDA) with step-wise addition of new variables was applied using SPSS (SPSS inc., Chicago, Illinois). The eight most discriminating texture features were selected according to the steepest descent in Wilks' lambda statistic. Leave-one-out was used as cross validation technique. These approaches were applied to each individual case, as well as on the pooled benign and malignant nuclei of all cases.

RESULTS

To perform the measurements took approximately 5 hr per patient sample, divided over acquisition, processing, manual intervention, and texture feature computation as follows: 45 min acquisition, 15 min automated segmentation, 2 hr of manual intervention, and 2 hr for the automated texture feature computation (total of 3 hr interaction). Figure 1 shows a maximum intensity projection from a representative image stack of a benign and a malignant prostate area. After segmenting the acquired image stacks we obtained 330 benign and 1,136 malignant nuclei. Figure 2 shows representative examples of benign and malignant nuclei. Table I shows the comparison between DNA ploidy status of the 3-D and conventional 2-D DNA histograms. The histograms were interpreted as we reported previously [16]. In all cases the DNA ploidy status was comparable, but the CV of the 3-D DNA histograms was higher. The selection of nuclei is quite different in the construction of the 2-D and 3-D DNA histograms. For the construction of the 2-D histograms, nuclei from both benign and malignant prostate regions are used, whereas only nuclei from a malignant region were selected for the 3-D histograms. Figure 3 shows the 2-D and 3-D DNA histograms for one representative case.

Table II shows the AUC values for 35 3-D nuclear texture features for discriminating between benign and malignant nuclei in the eight prostate cancer specimens, as well as AUC values for the combined dataset of 311 benign and 1,145 malignant nuclei. Five features did not show AUC values above 0.80. The best discriminating feature was average extinction ratio of low condensation state that showed AUC values ≥ 0.80 in six out of eight cases. AUC values for the pooled dataset were on average lower than for the individual cases.

TABLE I. Summary of Patient Data

		Number of cells		2-D image cytometry		3-D confocal DNA cytometry	
Case	Gleason score	Benign	Malignant	Ploidy	CV (%)	Ploidy	CV (%)
1	5	107	187	Tetraploid	13	Tetraploid	18
2	5	4	161	Diploid	7	Diploid	27
3	7	11	187	Diploid	7	Diploid	19
4	5	36	218	Diploid	6	Diploid	11
5	7	19	28	Diploid	8	Diploid	22
6	6	41	127	Diploid	5	Diploid	16
7	6	75	84	Diploid	7	Diploid	14
8	5	18	153	Diploid	7	Diploid	16

Gleason scores of the analyzed prostate cancers, the number of segmented benign and malignant cell nuclei and classification of the DNA histograms obtained by 2-D conventional image cytometry and 3-D confocal microscopy based DNA cytometry (measured on the malignant area) together with the CVs of the diploid peak.

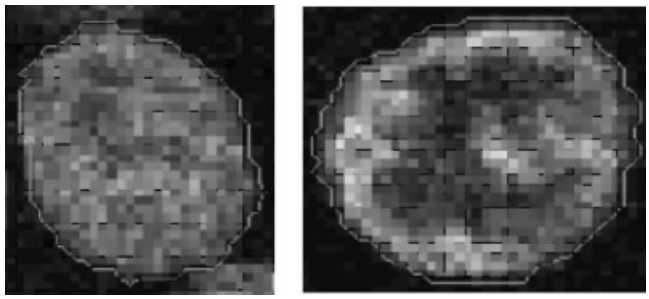

Fig. 2. Representative example of a section of a benign (**left**) and a malignant (**right**) nucleus. These nuclei are obtained from a stack of prostate tissue stained with TO-PRO-3, acquired by CLSM, imaged with a 100×/1.40 NA oil immersion objective. The differences in nuclear chromatin architecture are clearly visible (e.g., clumping of both bright and dark pixels, and wider range of pixel brightness in the malignant nucleus).

Table III shows the features selected in LDA (having a discriminant function co-efficient larger than 1) on the pooled dataset of benign and malignant nuclei of the eight specimens. Especially discrete texture features were able to discriminate between benign and malignant prostate tissue cell nuclei. The predictive performance (leaving-one-out corrected) of a linear discriminant function based on the eight selected 3-D nuclear texture features is shown in Table IV. Of the benign nuclei (N = 244), 76% were correctly classified, and 92% of the malignant nuclei (N = 1048) were correctly assigned to the malignant class.

DISCUSSION

The aim of this study was to perform a first evaluation of the discriminative power of 3-D nuclear DNA content and texture analysis in prostatectomy specimens containing prostate cancer after promising preliminary results in our previous study [17]. 3-D

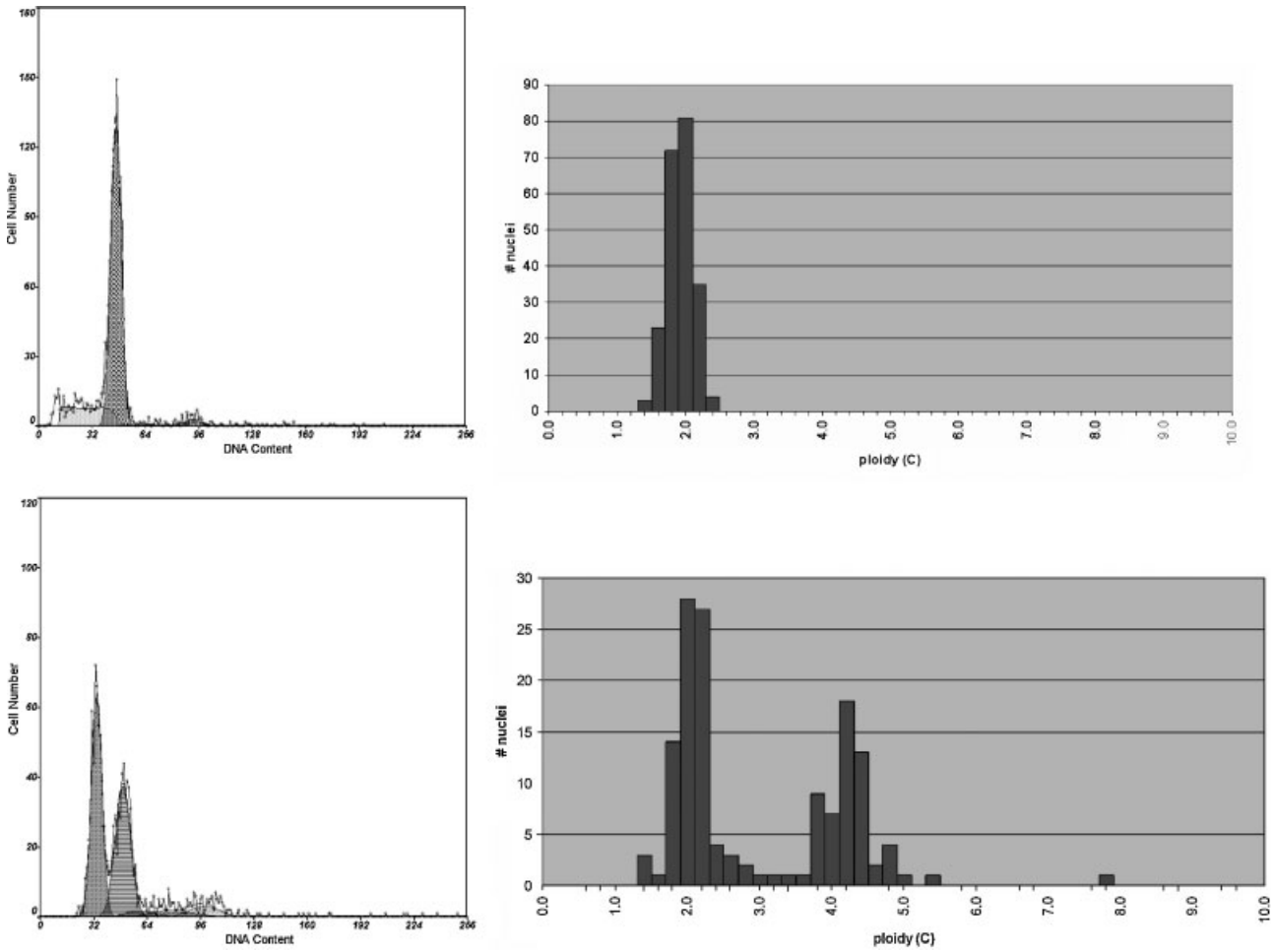

Fig. 3. DNA ploidy histograms for two selected cases of prostate adenocarcinoma as analyzed by conventional DNA image cytometry (**left**) and confocal laser scanning microscopy based 3-D image analysis (**right**). The first histograms are from a clearly diploid cell cycle. The second pair of histograms clearly has an aneuploid (about 3c) clone next to a population of about 2c nuclei.

TABLE II. AUC values for 35 3-D nuclear texture features

Case	1	2	3	4	5	6	7	8	All cases	# Features with AUC ≥0.80
Descriptive statistical features										
Sum of gray values	0.57	0.71	**0.93**	**0.95**	**0.87**	0.73	0.77	0.54	0.58	3
Mean of gray values	**0.88**	**0.91**	**1.00**	**0.82**	**0.87**	0.69	0.65	0.68	0.64	5
Variance of gray value distribution	0.68	0.80	**1.00**	0.61	0.55	0.53	0.62	0.59	0.62	1
Skewness of gray value distribution	0.79	**0.87**	**0.91**	**0.89**	0.67	**0.92**	0.57	0.55	0.60	4
Kurtosis of gray value distribution	0.70	0.75	0.71	**0.87**	0.62	**0.86**	0.61	0.54	0.56	2
Markovian texture features										
Energy	0.74	**0.88**	**0.98**	0.61	0.56	0.73	0.57	0.61	0.69	2
Entropy	0.65	0.76	**1.00**	0.55	0.59	0.58	0.51	0.53	0.56	1
Inverse difference moment	**0.88**	**0.86**	**1.00**	0.78	0.56	**0.83**	0.65	0.66	**0.81**	4
Contrast	**0.82**	**0.80**	**1.00**	0.71	0.51	0.73	0.61	0.57	0.75	3
Correlation	0.79	**0.88**	**1.00**	0.75	0.71	0.78	0.51	0.64	0.63	2
Cluster shade	0.53	0.60	0.71	0.51	0.57	0.62	0.50	0.54	0.53	0
Cluster prominence	0.62	**0.80**	**1.00**	0.58	0.55	0.57	0.50	0.58	0.60	2
Discrete texture features										
Pixel volume of low condensation state	0.65	0.52	**0.80**	**0.89**	0.53	0.79	0.57	0.70	0.67	2
Pixel volume of medium condensation state	0.73	0.80	**0.82**	0.71	0.61	**0.93**	0.56	0.70	0.71	2
Pixel volume of high condensation state	0.73	**0.83**	**0.83**	**0.84**	0.60	**0.90**	0.53	0.74	0.72	4
Average extinction ratio of low condensation state	**0.95**	**0.91**	**0.95**	**0.88**	**0.98**	**0.98**	0.57	0.59	0.56	6
Average extinction ratio of medium condensation state	0.75	0.75	0.74	0.52	0.78	0.53	0.54	0.59	0.52	0
Average extinction ratio of high condensation state	**0.86**	**0.87**	**0.87**	0.67	**0.94**	0.75	0.52	0.63	0.55	4
Low vs. medium average extinction ratio	**0.87**	0.50	**0.90**	0.79	**0.99**	**0.92**	0.60	0.59	0.55	4
Low vs. med-high average extinction ratio	**0.90**	0.68	**0.93**	**0.84**	**1.00**	**0.94**	0.59	0.58	0.51	5
Low vs. high average extinction ratio	**0.91**	0.76	**0.93**	**0.85**	**1.00**	**0.95**	0.58	0.59	0.50	5
# Unconnected parts of low condensation state	0.60	0.64	0.60	**0.82**	0.67	0.80	0.60	0.57	0.51	1
# Unconnected parts of medium condensation state	0.66	0.70	0.55	0.61	0.53	0.56	0.53	0.76	0.53	0
# Unconnected parts of high condensation state	0.58	0.68	0.56	0.72	0.80	0.66	0.64	0.63	0.61	0
Compactness of low condensation state	0.67	**0.95**	**1.00**	**0.93**	0.69	0.67	0.52	**0.90**	0.70	4
Compactness of medium condensation state	0.55	0.66	**0.95**	**0.83**	**0.81**	0.69	0.65	0.68	0.61	3
Compactness of high condensation state	0.53	0.64	**0.81**	0.65	0.69	0.62	0.62	0.61	0.55	1
Low average distinction genomic center	0.63	0.66	0.76	0.78	0.54	0.59	0.65	0.75	0.68	0
Medium average distinction genomic center	0.73	**0.86**	**0.85**	0.52	0.63	**0.93**	0.54	0.75	0.69	3
High average distinction genomic center	0.61	0.51	0.51	0.57	0.57	**0.89**	0.61	0.62	0.62	1
Low asymmetry nuclear center	0.65	0.56	0.77	**0.9**	0.55	0.78	0.57	0.70	0.66	1
Medium asymmetry nuclear center	0.73	0.77	0.78	0.72	0.63	**0.92**	0.56	0.71	0.70	1
High asymmetry nuclear center	0.72	0.77	0.79	**0.85**	0.62	**0.90**	0.54	0.74	0.72	2
Fractal texture features										
Lacunarity	0.63	0.58	0.79	0.54	0.54	**0.87**	0.64	0.75	0.58	1
Fractal dimension	0.59	0.69	0.78	0.66	0.57	**0.84**	0.61	0.72	0.65	1
# Features, AUC ≥ 0.80	8	12	22	14	8	15	0	1	1	6
# Benign nuclei	107	4	11	36	19	41	75	18	**311**	
# Malignant nuclei	187	161	187	218	28	127	84	153	**1145**	
Total number of nuclei	**294**	**165**	**198**	**254**	**47**	**168**	**159**	**171**	**1456**	

AUC values for 35 3-D nuclear texture features for discriminating between benign and malignant nuclei in eight prostate cancer specimens. In addition, the AUC values are shown for the combined dataset of 311 benign and 1,145 malignant nuclei. Texture feature values having an AUC value greater than 0.8 are indicated in bold.

nuclear texture features are a powerful tool in computer-aided diagnosis. This study is the first large-scale clinical study on 3-D nuclear texture features. The extra dimension compared to 2-D texture analysis previously described by others [8,24] gives more accurate discriminant functions [17].

The DNA ploidy status assessed in 3-D and conventional 2-D DNA histograms was similar.

TABLE III. Discriminant function coefficient of the selected 3-D texture features

Texture feature	Canonical discriminant function co-efficients	Texture feature
Category		
1. Gray skewness	1	General statistics
2. Energy	162	Markovian
3. Inverse difference moment	12	Markovian
4. Low average extinction ratio	76	Discrete
5. Medium average extinction ratio	25	Discrete
6. Low vs. medium average extinction ratio	2	Discrete
7. Low vs. medium-high average extinction ratio	1	Discrete
8. Medium asymmetry with respect to the nuclear center	2	Discrete

Absolute values of the discriminant function coefficients of the 3-D texture features selected in linear discriminant analysis to separate pooled benign and malignant nuclei from eight cases of prostate cancer. These co-efficients indicate their respective relevance in the discriminant analysis. The texture feature category is shown in the third column.

However, the CV of the 3-D DNA histograms was higher than in 2-D, in line with previous studies [15,16]. This can be explained by the lower number of analyzed nuclei and the problems with overlap in prostate tissue with principally very close lying cells relative to the resolution of the CLSM approach. Furthermore, the limited Z-resolution of the confocal microscope might contribute to this.

In univariate ROC analysis, several of the 3-D texture features could consistently discriminate between benign and malignant prostate nuclei in the different cases. By multivariate LDA of the pooled benign (N = 320) and malignant nuclei (N = 1,136), we were able to classify 76% of the benign and 92% of the malignant nuclei correctly. The imaged regions were thoroughly selected by a pathologist, and the benign areas were taken as far away as possible from the malignant areas. Nevertheless, we cannot exclude that some of the benign nuclei harbor subtle malignancy associated changes [12]. The large difference between the number of benign- and malignant-segmented nuclei is due to the difficulty of segmenting nuclei that are very close together or even overlapping in a tubular tissue structure.

Especially discrete texture features had high discriminative power. Clearly, no single feature has sufficient discriminatory power, so a multivariate approach using multiple features was necessary.

Although the segmentation procedure in our software has been automated to a high degree [14], prostate tissue (especially benign nuclei) still requires significant user interaction during segmentation due to the tight packing of especially benign nuclei. Software improvements are however on their way. We also expect further improvements from the increased Z-resolution of the new 4-pi confocal laser scanning microscopes [25] resulting in better images, or, by the use of deconvolution algorithms [26] which improve the Z-resolution of conventional CLSM images. Nevertheless, our approach has for the first time been proven to be clinically applicable and useful to detect prostate neoplasia. However, our results should be validated on more prostate cancer specimens. The limitations of this technique should be established by correlating texture feature changes to Gleason score and find the values for which discrimination is not possible anymore. Studying texture feature changes among neoplastic tissue other than prostate tissue should prove further clinical usefulness of this technique.

TABLE IV. Predictive performance of 3-D nuclear texture features using Linear Discriminant Analysis

	Predicted class membership					
Actual class	Benign		Malignant		Total	
Benign	244	76%	76	24%	**320**	**100%**
Malignant	88	8%	1,048	92%	**1,136**	**100%**

The predictive performance (leaving-one-out corrected) of a linear discriminant function based on the eight 3-D nuclear texture features assessed by CLSM. The features used for classification are depicted in Table III. The numbers indicate the amount (relative as well as absolute) of nuclei classified as being benign or malignant together with their actual group membership (as classified by a pathologist as our gold standard).

In conclusion, prostate cancer DNA histograms obtained by 3-D confocal microscopy were comparable to those obtained by conventional 2-D image cytometry. Although the number of patients is not very high, we have shown that quantification of changes in the distribution of nuclear chromatin by means of 3-D texture feature computation on images acquired by CLSM allows to correctly classify most benign and malignant prostate nuclei. This is further evidence that 3-D texture features are useful to discriminate between benign and malignant nuclei as reported in previous studies, although 3-D texture features are more sensitive to detect changes in nuclear chromatin architecture than 2-D texture features.

REFERENCES

1. Zink D, Fischer AH, Nickerson JA. Nuclear structure in cancer cells. Nat Rev Cancer 2004;4:677–687.
2. Mommers EC, Poulin N, Meijer CJ, Baak JP, van Diest PJ. Malignancy-associated changes in breast tissue detected by image cytometry. Anal Cell Pathol 2000;20:187–195.
3. Bergers E, Baak JP, van Diest PJ, Willig AJ, Los J, Peterse JL, Ruitenberg HM, Schapers RF, Somsen JG, van Beek MW, Bellot SM, Fijnheer J, van Gorp LH. Prognostic value of DNA ploidy using flow cytometry in 1301 breast cancer patients: Results of the prospective Multicenter Morphometric Mammary Carcinoma Project. Mod Pathol 1997;10:762–768.
4. Veltri RW, Partin AW, Miller MC. Quantitative nuclear grade (QNG): A new image analysis-based biomarker of clinically relevant nuclear structure alterations. J Cell Biochem Suppl 2000; Suppl 35:151–157.
5. Guillaud M, Doudkine A, Garner D, Macaulay C, Palcic B. Malignancy associated changes in cervical smears: Systematic changes in cytometric features with the grade of dysplasia. Anal Cell Pathol 1995;9:191–204.
6. Bartels PH, Montironi R, Hamilton PW, Thompson D, Vaught L, Bartels HG. Nuclear chromatin texture in prostatic lesions. I. PIN and adenocarcinoma. Anal Quant Cytol Histol 1998;20:389–396.
7. Bartels PH, Montironi R, Hamilton PW, Thompson D, Vaught L, Bartels HG. Nuclear chromatin texture in prostatic lesions. II. PIN and malignancy associated changes. Anal Quant Cytol Histol 1998;20:397–406.
8. Palcic B. Nuclear texture: Can it be used as a surrogate endpoint biomarker? J Cell Biochem Suppl 1994;19:40–46.
9. Bartels PH. Computer-generated diagnosis and image analysis. An overview. Cancer 1992;69:1636–1638.
10. Veltri RW, Khan MA, Miller MC, Epstein JI, Mangold LA, Walsh PC, Partin AW. Ability to predict metastasis based on pathology findings and alterations in nuclear structure of normal-appearing and cancer peripheral zone epithelium in the prostate. Clin Cancer Res 2004;10:3465–3473.
11. Verhagen PC, Tilanus MG, de Weger RA, van Moorselaar RJ, van den Tweel JG, Boon TA. Prognostic factors in localised prostate cancer with emphasis on the application of molecular techniques. Eur Urol 2002;41:363–371.
12. Mairinger T, Gschwendtner A. Nuclear chromatin texture analysis of nonmalignant tissue can detect adjacent prostatic adenocarcinoma. Prostate 1999;41:12–19.
13. Tekola P, Baak JP, van Ginkel HA, Belien JA, van Diest PJ, Broeckaert MA, Schuurmans LT. Three-dimensional confocal laser scanning DNA ploidy cytometry in thick histological sections. J Pathol 1996;180:214–222.
14. Belien JA, van Ginkel AH, Tekola P, Ploeger LS, Poulin NM, Baak JP, van Diest PJ. Confocal DNA cytometry: A contour-based segmentation algorithm for automated three-dimensional image segmentation. Cytometry 2002;49:12–21.
15. Ploeger LS, Belien JA, Poulin NM, Grizzle W, van Diest PJ. Confocal 3D DNA cytometry: Assessment of required coefficient of variation by computer simulation. Cell Oncol 2004;26: 93–99.
16. Ploeger LS, Huisman A, van der GJ, van der Giezen DM, Belien JA, Abbaker AY, Dullens HF, Grizzle W, Poulin NM, Meijer GA, van Diest PJ. Implementation of accurate and fast DNA cytometry by confocal microscopy in 3D. Cell Oncol 2005;27: 225–230.
17. Huisman A, Ploeger LS, Dullens HF, Poulin N, Grizzle WE, van Diest PJ. Development of 3D chromatin texture analysis using confocal laser scanning microscopy. Cell Oncol 2005;27:335–345.
18. Suzuki T, Fujikura K, Higashiyama T, Takata K. DNA staining for fluorescence and laser confocal microscopy. J Histochem Cytochem 1997;45:49–53.
19. Ploeger LS, Gugten J, van der Giezen D, Belien JA, Abbaker A, Dullens HFJ, Huisman A, Grizzle W, Poulin N, van Diest PJ. Implementation of routine confocal DNA cytometry of clinical samples in 3D. Cell Oncol 2005;27:152.
20. Haroske G, Baak JP, Danielsen H, Giroud F, Gschwendtner A, Oberholzer M, Reith A, Spieler P, Bocking A. Fourth updated ESACP consensus report on diagnostic DNA image cytometry. Anal Cell Pathol 2001;23:89–95.
21. Doudkine A, Macaulay C, Poulin N, Palcic B. Nuclear texture measurements in image cytometry. Pathologica 1995;87:286–299.
22. Metzler V, Palm C, Lehmann T, Aach T. Texture Classification of Graylevel Images by Multiscale Cross-Cooccurrence Matrices. 2000. p 2549.
23. Chaudhuri BB, Sarkar N. Texture segmentation using fractal dimension. IEEE Trans Pattern Anal Machine Intell 2005;17: 72–77.
24. Bartels PH, da Silva VD, Montironi R, Hamilton PW, Thompson D, Vaught L, Bartels HG. Chromatin texture signatures in nuclei from prostate lesions. Anal Quant Cytol Histol 1998;20:407–416.
25. Schrader M, Bahlmann K, Giese G, Hell SW. 4Pi-confocal imaging in fixed biological specimens. Biophys J 1998;75:1659–1668.
26. Markham J, Conchello JA. Artefacts in restored images due to intensity loss in three-dimensional fluorescence microscopy. J Microsc-Oxf 2001;204:93–98.